Synthesis and cellular characterization of various nano-assemblies of cell penetrating peptide-epirubicin-polyglutamate conjugates for the enhancement of antitumor activity

Article (Accepted Version)

Synthesis and cellular characterization of various nano-assemblies of cell penetrating peptides-epirubicin-polyglutamate conjugates for enhancement of antitumor activity

Samaneh Mohammadi[1], Parvin Zakeri-Milani[2], Nasim Golkar[3,4], Samad Mussa Farkhani[1,5], Ali Shirani[1,5], Javid Shahbazi Mojarrad[2], Ali Nokhodchi[6], Hadi Valizadeh[7*]

Affiliations:

[1]Biotechnology Research Center and Faculty of Advanced Medical Sciences, Tabriz University of Medical Sciences, Tabriz, Iran.

[2]Liver and Gastrointestinal Diseases Research Center and Faculty of Pharmacy, Tabriz University of Medical Sciences, Tabriz, Iran.

[3]Pharmaceutics Department, School of Pharmacy, Shiraz University of Medical Sciences, Shiraz, Iran.

[4]Pharmaceutical Science Research Center, Shiraz University of Medical Science, Shiraz, Iran.

[5]Student Research Committee, Tabriz University of Medical Sciences, Tabriz, Iran.

[6]Pharmaceutics Research Laboratory, School of Life Sciences, University of Sussex, Arundel Building, Brighton BN1 9QJ, UK.

[7]Drug Applied Research Center and Faculty of Pharmacy, Tabriz University of Medical Sciences, Tabriz, Iran.

*To whom correspondence should be addressed:

Dr. Hadi Valizadeh, PharmD, PhD, Professor,

Drug Applied Research Center and Faculty of Pharmacy, Tabriz University of Medical Sciences, Tabriz, Iran. 51664.

E-mail: valizadeh@tbzmed.ac.ir

Phone: +98 (41) 3339-2649

Fax: +98 (41) 3334-4798

Synthesis and cellular characterization of various nano-assemblies of cell penetrating peptides-epirubicin-polyglutamate conjugates for enhancement of antitumor activity

Abstract

A new class of cell penetrating peptides (CPPs) named peptide amphiphile was designed to improve the intracellular uptake and antitumor activity of epirubicin (EPR). Various amphiphilic CPPs were synthesized by solid phase peptide synthesis method and were chemically conjugated to EPR. Their corresponding nanoparticles (CPPs-E4 and CPPs-E8) were prepared via non-covalent binding of the peptides and polyanions. Cytotoxicity and anti-proliferative activity were evaluated by MTT assay. Cellular uptake was examined by flow cytometry and fluorescence microscopy. The CPPs exhibited slight cytotoxicity. Binding of polyglutamate to CPPs (CPPs-E4 and CPPs-E8 nanoparticles) decreased their cytotoxicity. CPPs-E8 nanoparticles showed lower cytotoxicity than CPPs-E4 nanoparticles. Cellular uptake of K3W4K3-E8, K2W4K2-E8 and W3K4W3-E8 reached 100% with no difference between each of the mentioned CPPs and its nanoparticle at 50 µM. The anti-proliferative activity of EPR was enhanced following conjugation to peptides and nanoparticles at 25 µM. CPPs-EPR-E4 and –E8 nanoparticles displayed higher anti-proliferative activity than CPPs-EPR at 25 µM. CPPs–E8-EPR nanoparticles showed higher anti-proliferative activity than CPPs–E4-EPR. K3W4K3-E8-EPR nanoparticles exhibited the highest anti-proliferative activity at 25 µM. The synthesized peptide nanoparticles are proposed as suitable carriers for improving the intracellular delivery of EPR into tumor cells with low cytotoxicity and high antitumor activity.

Key words: Cell penetrating peptides, epirubicin, solid phase peptide synthesis, glutamate, nanoparticles, drug delivery

1. Introduction

Despite vast advances about anticancer drugs during the last decade, cancer is still one of the important worries of the world [1, 2]. Ineffective accumulation of drugs in tumors, lack of tumor specificity, heterogeneity of cancer cells, drug toxicity and drug resistance are factors that causes the lack of efficiency in cancer therapy [1, 3, 4].

Epirubicin (EPR) is an anthracycline drug that has been used alone or in combination with other drugs for treatment of various cancers such as breast, ovarian, gastric and lung [5, 6]. EPR is a stereoisomer of doxorubicin and is flavoured over it. It has been shown that EPR is generally more successful than doxorubicin due to the higher tumor therapeutic efficiency and less side effects [7, 8]. In fact, as a consequence of the reorientation of the hydroxyl group in the 4'-position of the daunosamine ring, epirubicin finds different pharmacologic properties than doxorubicin [9]. First, it has a lower pKa. Accordingly, it is more lipophilic and better able to penetrate cells. Second, the glucuronidation of epirubicin and epirubicinol to inactive metabolites leads to a shorter terminal half-life for epirubicin (30 hours) compared with doxorubicin (45 hours) [8, 9]. Third, higher doses of epirubicin are required to produce the same degree of toxicity as doxorubicin. The doxorubicin-epirubicin dose ratios for similar toxicities are 1:1.2 for hematologic, 1:1.5 for nonhematologic, and 1:1.8 for cardiac [8, 10].

Although EPR exhibited activity in all phases of the cell cycle but it was active mostly in S and G2 phases. The antineoplastic effect of epirubicin occurs through a number of mechanisms. First, it intercalates between DNA nucleotide base pairs, resulting in the inhibition of DNA, RNA, and protein synthesis. Second, the intercalation leads to topoisomerase II cleavage of DNA, which results in cytocidal activity. Third, epirubicin inhibits DNA helicase activity, which ultimately interferes with replication and transcription [10, 11]. Various experiments have shown that EPR inhibits cell proliferation and DNA synthesis in various carcinoma cell lines. Although fewer, like chemotherapy drugs, EPR still

shows side effects such as cardio toxicity and myelosuppression [7]. Development of resistance to a certain dose of anticancer drugs is another major limitation of EPR. EPR is a hydrophilic drug with high volume of distribution [11].

Drug delivery systems modify the efficacy and toxicity of anticancer drugs. Moreover, drug delivery systems can avoid multi drug resistance (MDR) created through factors such as P-glycoprotein and multi drug resistance proteins (MRPs) [12, 13, 14, 15, 16, 17]. Chemical conjugation with a parent drug as "Prodrug" strategy is one of the drug delivery systems that has been widely used in EPR delivery [12]. Several methods have been used to improve EPR delivery, including using nanodiamond [18], SLN (solid lipid nanoparticles) [19], phospholipids as multi drug resistance modulators of the epirubicin transport [20], carbon nanoparticles [21], and PLGA nanoparticles [22].

Peptides and proteins are generally worthy in many aspects, such as their possible high potency, good selectivity and acceptable toxicity [23]. Two decades ago, a new kind of peptides, commonly known as cell penetrating peptides (CPPs), was discovered. They have been extracted from natural proteins and have the capability to cross cellular membranes and mediate the uptake of a wide range of macromolecular cargoes [1, 24, 25, 26, 27]. The discovered peptides as non-invasive vectors with very limited toxicity introduced a novel field in drug delivery [28]. In addition, they can be modified or designed de novo. They are typically short; usually 5–30 amino acids long [27, 29, 30, 31, 32, 33, 34]. These bioactive and biodegradable peptides are able to carry and deliver their cargoes such as nucleic acids, proteins, drugs, or imaging agents, to the cytoplasm or nuclei of cells [29, 32, 33, 34]. In the recent years, numerous natural and synthetic CPPs such as polyarginines, TAT (trans-acting activator of transcription) [26] and peptide amphiphiles (PA) [22] have improved the cellular uptake of various drugs such as Taxol [35], methotrexate [16], and doxorubicin [12]. Among these CPPs, peptide amphiphiles appear to be among efficient systems in drug delivery [36,

37, 38]. Universally, peptide amphiphiles consist of hydrophobic segments such as tryptophan and charged segments such as arginine or lysine [36]. These peptides have a helical secondary structure with the hydrophobic and hydrophilic domains. They use the charged region for cell membrane interaction and the hydrophobic region for membrane perturbation and translocation [29, 39]. Moreover, several studies have shown that the presence of tryptophan and backbone spacing can affect the uptake efficiency as well as its mechanism [40].

In the present study several novel CPPs based on different designs containing lysine and tryptophan were synthesized. Highly active EPR (instead of Doxorubicin) was utilized as a drug. These peptides were then conjugated to EPR to improve the antitumor activity of the drug in MCF-7 breast cell line. Their corresponding nano-assemblies were prepared by non-covalent binding of the peptides and polyglutamate, with two different chain lengths. Finally, cytotoxicity, intracellular uptake and antitumor activity of the synthesized peptides as well as their nanoparticles were investigated and compared.

2. Materials and Methods

2.1. Materials

Classical glass reaction vessels suitable for performing solid-phase peptide synthesis (SPPS) were made by glassblowers. All of the amino acids (lysine, tryptophan and glutamate) and Rink amid-resin were purchased from Aapptec [15]. N, N, N′, N′-Tetramethyl-O-(benzotriazol-1-yl) uraniumtetrafluoroborate (TBTU) and N,Ndiisopropylethylamine (DIPEA) as coupling reagents, dichloromethane (DCM) and N,N dimethyl formamide (DMF) as activating reagents, phenol and triisopropylsilane (TIS) as scavengers, trifluoroacetic acid (TFA), fluorescein isothiocyanate (FITC), 3-(4,5-Dimethylthiazol-2-yl)-2,5-diphenyltetrazolium bromide (MTT) and dimethyl sulfoxide (DMSO) were all obtained from

Sigma-Aldrich [15]. Potassium cyanide (KCN), ninhydrin and pyridine were from Merck (Germany). MCF-7 cells were purchased from Pasteur Institute (Iran).

2.2. Synthesis of peptides

Six linear peptides named (KW)4, (KW)5, K3W4K2, K3W4K3, W2K4W2 and W3K4W3 were synthesized using the hydrophobic (tryptophan, W) and charged (lysine, K) amino acids with various designs as presented in Table 1. Overall methods were carried out according to the previously reported procedure [36, 41, 42]. Briefly, all peptides were synthesized manually by solid-phase peptide synthesis method, assembled on Rink-Amide AM resin by Fmoc strategy using a fritted glass vessel. Fmoc-Rink amide resin (0.049 mmol, 0.3 mmol/g) was swollen in DMF for approximately 1 h under dry nitrogen. Fmoc groups at N-terminal of the linear peptide sequence of resin were removed using piperidine in DMF (20% v/v, total volume of 2 ml). Following a 30-min incubation at room temperature, Fmoc-Lys (Boc)-OH or Fmoc-Try (Boc)-OH (0.148 mmol) was coupled to the N-terminal of Rink amide resin in the presence of TBTU (0.148 mmol) and DIPEA (0.148 mmol) in DMF (2 ml) by mixing for 1.5 h. Completion of coupling was confirmed by Kaiser Test. The reaction solution was filtered off. Then, the obtained resin was washed with DMF (3 times each with 2 ml) and DCM (3 times each with 2 ml) and dried under vacuum overnight. Following the drying process, a fresh cleavage cocktail composed of TFA:phenol:water:TIS (88:5:5:2 v/v/v/v, total mixture volume of 10 ml per 100 mg peptide) was added to the resin. After shaking the mixture at room temperature for 2 h, the resin was collected and washed with another 2 ml fresh cleavage cocktail. The medium of the combined filtrates were evaporated and reduced into a minimum volume using dry nitrogen. The crude unreacted peptide was precipitated by adding excess volume (ten-fold) of cold diethyl ether and centrifugation at 4000 rpm for 5 min. Finally, the product was further washed with diethyl ether (50 ml) twice and then lyophilized. The schematic peptide synthesis of K3W4K3 is illustrated in Figure 1a.

2.3. Fluorescent labeling of the peptides on the resin

Fmoc protecting group was removed from N-terminal of all synthesized peptides using piperidine solution in DMF (20%, 2 ml, 30 min). A solution of 1/1 equivalent of FITC was provided in pyridine/DMF/DCM (12:7:5). Then FITC was attached to the peptides through adding the above solution to the resin-peptides (0.049 mmol) followed by an overnight mixing. The FITC-labeled peptides were evaluated by Kaiser Test to confirm the success of labeling process [42]. The schematic synthesis of FITC-labeled K3W4K3 is demonstrated in Figure 1b.

2.4. Preparation of nanoparticles

Peptide nanoparticles were synthesized by conjugation of the linear peptides to polyglutamate (E), with two chain lengths of E4 (EEEE) and E8 (EEEEEEEE). The synthesized linear peptides dissolved in DMSO were added to the polyglutamate E4 and E8 solution in DMSO, at different proportions of 1:1, 1:5 and 1:10 (v/v). Then, the prepared peptide solutions were sonicated so that the nanoparticles were formed through self-assembly by electrostatic attraction.

2.5. Determination of particle size

Morphology and size of the synthesized CPPs and nanoparticles were investigated by scanning electron microscopy (SEM). Each sample was dissolved in DMSO and distilled water (1:99 v/v), dropped onto an aluminum plate and lyophilized. The prepared slides were then visualized using a Philips XL electron microscope.

2.6. Preparation of peptide-drug conjugates

Conjugates of peptide-drug (CPP-EPR for various CPPs) were synthesized through reaction of amine group in peptide and hydroxyl group in EPR drug using a succinyl spacer. When succinic anhydride binds to the peptides as a linker, NH_2 group of the peptide is changed to a carboxyl moiety. N-terminal of the prepared peptides was deprotected using piperidine in

DMF (20%). Then the deprotected peptides were treated with succinic anhydride (1.5 eq) and DIEPA (3 eq) in DMF for 2 h. The completion of the reaction was confirmed by the Kaiser Test. Following washing the resin with DMF (3 ×2 ml) and DCM (3× 2 ml), DIEPA (0.25 ml, 1.44 mmol) was added dropwise to the mixture of succinylated peptide and TBTU (3 eq) in DMF (2 ml) under stirring for 30 min. Afterward, EPR (1/5 eq) solution in DMF (2 ml) was added to the above mixture. The reaction mixture was stirred at room temperature for 48 h. Following drying using nitrogen gas, peptide-EPR conjugates were cleaved from the resin with cleavage cocktail composed of TFA/phenol/water/Tis (88:5:5:2 v/v/v/v, total volume of 10 ml per 100 mg peptide). Then, the corresponding nanoparticles (CPP-E4-EPR and CPP-E8-EPR each for various CPPs) were prepared similarly as mentioned in the section 2.4. The schematic synthesis of K3W4K3-EPR conjugate is shown in Figure 1c.

2.7. Drug loading measurement

UV spectra were obtained in order to evaluate the conjugation of EPR to various CPPs using a UV spectrophotometer. Afterward, absorbance of the unreacted EPR for each sample and the standard solution (first EPR concentration) were measured at the wavelength of 504 nm. Loading of EPR (%) was calculated from Equation (1).

$$Drug\ loading\ \% = 1 - \frac{A_f}{A_s} \times 100 \quad \text{Equation (1)}$$

Where A_f and A_s represent the optical absorbance of the sample and the standard, respectively.

2.8. Cell culture

Cellular studies were performed using MCF-7 (human breast adenocarcinoma) cell line. The cells were cultured on cell culture flasks in RPMI 1640 medium supplemented with 10% fetal bovine serum (FBS; Gibco, USA) and 1% antibiotic–antimycotic (Penicillin–Streptomycin; Gibco, USA) in an incubator (5% CO_2) at 37 °C.

2.9. Cytotoxicity and anti-proliferative assay

The MTT assay was carried out to evaluate and compare the cytotoxicity and anti-proliferative activity of various samples (different CPPs, CPPs-E4 and –E8 nanoparticles for cytotoxicity; different CPPs, CPPs-EPR, CPPs-E4-EPR, CPPs- E8-EPR and EPR alone for anti-proliferative activity) each at different concentrations. MCF-7 cell suspension at a density of 2×10^4 cells/well was seeded into 96-well microplates. Following incubation at 37 ºC and 5% CO_2 for 24 h and medium aspiration, the cells were treated with the 1/10 diluted samples in serum-free culture medium each at different final concentrations of 5, 10 and 25 µM for cytotoxicity and 1, 5, 10 and 25 µM for anti-proliferative assay. The cells were incubated for 24 h or 48 h, and then the medium was aspirated and replaced with 50 µl of MTT solution (2 mg/ ml). After 4 h incubation, the medium was aspirated again and insoluble formazan crystals in each well were dissolved in mixture of dimethyl sulfoxide (DMSO, 200 µl) and Sorensen's phosphate buffer (25 µl). The absorbance was measured by a microplate reader (Bio-Tek, USA) at a wavelength (λ) of 570 nm with reference to 650 nm. All of the results were blank corrected. The experiment was run for 6 replicates. Anti-proliferative activity was calculated according to Equation (2).

$$Anti-proliferative\ activity\ (\%) = \left(1 - \frac{AS570 - AS650}{AC570 - AC650}\right) \times 100 \quad \text{Equation (2)}$$

Where AS_{570} and AS_{650} correspond to the absorbance of treated samples at the respective λ = 570 and 650 nm; AC_{570} and AC_{650} are the corresponding absorbance of untreated control cells.

2.10. Fluorescence microscopy

The cellular uptake of CPPs and the corresponding nanoparticles were visualized using fluorescence microscopy. MCF-7 cells were seeded on the coverslips placed inside the six

well plates at a density of 1×10^5 cells per well and incubated at 37 ºC and 5% CO_2 for 24 h. Then, the cells were treated with the FITC-CPPs and FITC-CPPs-E8 nanoparticles in serum-free culture medium each at the concentration of 10, 25 and 50 μM and incubated for 2 h. Subsequently, the medium of each well was aspirated and the cells were washed three times with cold phosphate buffered saline (PBS). For fixing the cells, 200 μl of 2% formaldehyde solution in PBS was added to each well and incubated at 37 °C for 15 min followed by washing three times with PBS. Then, the samples were visualized by a fluorescence microscope (Olympus IX81, Olympus Optical Co. Ltd., Japan).

2.11. Cell uptake quantification by flow cytometry

For cellular uptake quantification, flow cytometry assay was performed. MCF-7 cells were seeded in 6-well plates at a density of 2×10^5 cells/well and incubated at 37 ºC and 5% CO_2 for 24 h. Following culture medium aspiration and washing with PBS, the cells were treated with FITC-CPPs and FITC-CPPs-E8 nanoparticles in serum-free culture medium each at concentrations of 10, 25, and 50 μM. After 2 h incubation at 37 °C, the cells were washed three times with PBS and detached from the well by 3-min incubation at 37 °C with 0.53 mM of 0.25% trypsin/EDTA. Then, the cells were harvested, centrifuged, resuspended in 0.5 ml cold PBS and homogenized by pipetting several times. The cells were kept on ice until measurement of the treated cell-associated fluorescence intensity of FITC at the emission wavelength of 519 nm through FL1 channel for total of 10,000 events (cells/sample) using a FACSCalibure flow cytometer (Becton, Dickinson, USA). Cell Quest software (Becton, Dickinson, USA) was used for data acquisition. The analysis of fluorescence intensities was performed subsequently via the above mentioned software for the gated singlet cells.

2.12. Statistical analysis

The data were expressed as mean ± standard deviation of 3 to 6 determinations. Statistical analysis was performed using Graphpad Prism Software Inc. version 5.04 (Inc. La Jolla, CA,

USA). Different samples were compared using two-way analysis of variance (ANOVA). The differences were quoted statistically significant where $P < 0.05$. The significance level for pair wise comparisons was adjusted by Bonferroni method using Student t-test.

3. Results

Different linear peptides were synthesized on the Rink amide resin. Peptide synthesis was confirmed using Kaiser Test. In the next step, FITC was coupled to the synthesized peptides to investigate their uptake efficiency. FITC labeling was also confirmed by Kaiser Test. CPPs-Drug conjugates (CPPs-EPR) were then prepared using a succinic linker. CPPs, FITC-CPPs and CPPs-EPR were cleaved from the resin using the cleavage cocktail. EPR conjugation to CPPs and EPR loading were evaluated by UV spectrophotometry. Afterward, peptide nanoparticles were synthesized by conjugation of the peptides to poly glutamate (E), with two chain lengths, E4 and E8. Different synthesized CPPs and the corresponding nanoparticles were finally characterized by scanning electron microscopy (supplementary data, Figure S1), cytotoxicity, cellular uptake and anti-proliferative activity

3.1. Cytotoxicity

As an efficient delivery vector of anti-cancer drugs, blank CPPs and nanoparticles must have low levels of toxicity against cells. Therefore, the cytotoxicity of all synthesized CPPs and the corresponding nanoparticles (E4 and E8) were evaluated in MCF-7 cancer cells as a function of concentrations (5, 10 and 25 µM) after 24 and 48 h incubation time. For blank peptides, i.e. CPPs, cytotoxicity was concentration dependent ($P<0.001$). The toxicity results for all of the nanoparticles showed that an increase in the concentration of peptides resulted in an increase in the toxicity after incubation for 24 (supplementary data, Figure S2) and 48 h (Figure 2). The increase in the toxicity of nanoparticles found to be statistically significant ($P<0.0001$). Following 24 h of incubation of the peptides with MCF-7 cells, all of the CPPs showed low cytotoxicity (< 20%) at the concentration of 5 µM. (KW)5, K2W4K2 and

W3K4W3 showed the lowest cytotoxicity (16%, 21% and 22%, respectively) at the concentration of 10 µM ($P<0.001$). In addition, at the highest concentration (25 µM), cytotoxicity of W3K4W3 was the lowest (22%) followed by (KW)5 and K3W4K3 peptides (32% and 35%, $P < 0.00001$). Incubation time also affected the cytotoxicity of the peptides. Increasing the incubation time from 24 (supplementary data, Figure S2) to 48 h (Figure 2) resulted in higher cytotoxicities ($P < 0.0001$). As illustrated in Figure 2a, (KW)5 showed the lowest cytotoxicity at concentration of 5 µM (15%, $P < 0.01$). The lowest cytotoxicity was observed for K2W4K2 and K3W4K3 (25% and 26%, $p < 0.001$) when the concentration was 10 µM. In the cases of (KW)5 and K3W4K3 (42% and 42%, $P < 0.01$) the lowest toxicity was obtained at 25 µM. Binding of E4 to peptides led to a significant reduction in the cytotoxicity at different concentrations for both 24 ($P<0.0001$) and 48 h ($P<0.001$) incubation times (Figure 2b). As demonstrated in Figure 2c, binding of E8 to peptides also resulted in a significant decrease in the cytotoxicity at different concentrations for all nanoparticles at the both incubation times, 24 and 48 h ($P < 0.00001$ and $P < 0.0001$). Interestingly, CPPs-E8 nanoparticles showed lower cytotoxicity than CPPs-E4 nanoparticles ($P < 0.001$). Therefore, CPPs-E8 nanoparticles possessed the lowest cytotoxicity among all nanoparticles. All of CPPs-E8 nanoparticles showed very low cytotoxicity (<20%) even at the highest concentration (25 µM) except (KW)4-E8 (at 10 and 25 µM) and K2W4K2-E8 (just at 25 µM).

3.2. Cellular uptake by fluorescence microscopy

Thecellular uptake (intracellular localization) was first visualized by fluorescent microscopy. MCF-7 cells were incubated with various FITC-CPPs and FITC-CPPs-E8 at concentrations of 10, 25, and 50 µM for 2 h. As illustrated in Figure 3, cell treatments with high level concentrations of the samples (25 µM, supplementary data Figure S3; and 50 µM, Figure 3) led to increase the cellular uptake in comparison with lower concentration (10 µM, Figure 3)

for both CPPs and nanoparticles. Besides, it was indicated that CPPs and CPPs-E8 nanoparticles of K3W4K3, W3K4W3, (KW)5 and (KW)4 accumulated in the nucleus of the cells, while K2W4K2 peptide and its corresponding nanoparticle localized in the cytoplasm. It was demonstrated that W2K4W2 (both peptide and its nanoparticles) had the lowest cellular uptake.

3.3. Cellular uptake by flow cytometry

Flow cytometry was performed in order to evaluate and compare the cellular uptake ability of different peptides and their nanoparticles (FITC-CPPs and FITC-CPPs-E8 nanoparticles). Just like fluorescence microscopy, MCF-7 cells were incubated with different concentrations of the samples for 2 h at 37 ºC. As shown in Figure 4, the uptake was concentration dependent for all of the CPPs and nanoparticles. In other words the percentage of cellular fluorescence increased with increasing the concentration up to 25 µM ($P<0.0001$). At this concentration, the cell fluorescence reached the maximum percentage (about 100%) for all of the CPPs except W2K4W2 (Figure 4d) which was very low (about 20%). By increasing the concentration from 25 µM to 50 µM, the cell fluorescence remained stable (at plateau) for K3W4K3 (Figure 4a), W3K4W3 (Figure 4b) and K2W4K2 (Figure 4c). However, in the case of (KW)4 (Figure 4e) and (KW)5 (Figure 4f) the cell fluorescence decreased to about 75%. Among all of the CPPs, W2K4W2 (Figure 4d) exhibited the lowest uptake ($P < 0.00001$). For all of the nanoparticles (Figure 4), cellular uptake was lower compared to their corresponding CPPs at the concentration of 10 µM ($P < 0.0001$) and 25µM ($P < 0.001$). The fluorescent signal of K3W4K3-E8 (Figure 4a), K2W4K2-E8 (Figure 4b) and W3K4W3-E8 (Figure 4c) reached the same percentage with the corresponding CPPs, i.e. the maximum percentage of approximately 100% at the concentration of 50 µM and there was no significant difference between each of the mentioned CPPs and its nanoparticle ($P>0.05$). Cellular uptake of (KW)4-E8 (Figure 4e) and (KW)5-E8 (Figure 4f) was significantly higher in comparison

with their corresponding CPPs at the concentration of 50 μM ($P < 0.0001$ for both). Although, the cell uptake of W2K4W2-E8 (Figure 4d) was significantly higher than its corresponding CPP (W2K4W2) at the concentrations of 25 μM ($P < 0.0001$) and 50 μM ($p < 0.0001$), it still exhibited the lowest percentage of cellular uptake compared to all other CPPs-E8 nanoparticles ($P<0.00001$). Flow cytometry histograms of K3W4K3 and K3W4K3-E8 each at various concentrations of 10, 25 and 50 μM are presented in Figure 5.

3.4. Drug loading measurement

Following the conjugation of EPR to different CPPs, conjugation was confirmed using UV spectrophotometry (supplementary data, Figure S4).

3.5. Antitumor activity of drug loaded CPPs

To determine whether the synthesized peptides and nanoparticles can be utilized for delivery of biologically relevant doses of EPR to cells, EPR was conjugated to them and the antitumor (anti-proliferative) activity of EPR was then examined and compared in MCF-7 cells at various concentrations. As illustrated in Figure S5a (24 h, supplementary data) and Figure 6 (48 h), even the low concentration of 1 μM resulted in a significant increase in antitumor activity. As demonstrated in Figure 6 (48 h), anti-proliferative activity was concentration dependent which increased by increasing the concentration ($P<0.001$). Moreover, incubation time also led to higher anti-proliferative activity ($P < 0.01$, supplementary data, Figure S5 for 24h; Figure 6 for 48h). Following the conjugation of EPR to the CPPs, CPPs-E4 and CPPs-E8 nanoparticles, the anti-proliferative activity of the drug increased significantly ($P<0.001$) at the highest concentration (25 μM). Free drug (EPR) showed 63% anti-proliferative activity (37% cell viability) at the concentrations of 25 μM. The anti-proliferative activity increased to 64%-79% and 77%-91% (Figure 6a) for all CPPs-EPR conjugates at 25 μM at the respective incubation times of 24 ($P< 0.05$, supplementary data, Figure S5a) and 48 h ($P < 0.01$, Figure 6a). Among the six CPP-EPR conjugates at 25 μM concentration, K3W4K3-

EPR exhibited the highest anti-proliferative activity (80%) and W2K4W2-EPR as well as (KW)4-EPR possessed the lowest anti-proliferative activity (62%) after 24 h incubation (supplementary data, Figure S5a). Following the increase of incubation time to 48 h at 25 µM concentration, K3W4K3-EPR and W2K4W2-EPR showed the highest (90%) and the lowest (74%) anti-proliferative activity, respectively, as demonstrated in Figure 6a. CPPs-EPR-nanoparticles displayed higher anti-proliferative activity compared to CPPs-EPR conjugates ($p<0.05$) at both incubation times especially at higher concentrations. Among all CPPs-EPR-nanoparticles, CPPs–E8-EPR (Figure S5c (supplementary data) and Figure 6c) showed higher anti-proliferative activity than CPPs–E4-EPR (Figure S5b (supplementary data) and Figure 6b) at both incubation times ($P<0.05$ and $P<0.01$). As illustrated in Figure 6c, K3W4K3-E8-EPR nanoparticles exhibited the highest anti-proliferative activity (92%) for all CPPs-E8-EPR at 25 µM following incubation for 48 h ($P < 0.05$).

4. Discussion

Coupling of EPR to CPPs has been employed as one of the specific methods to deliver drug molecules into various cell lines. In the present study, different peptide sequence designs were chosen for peptide synthesis to examine how the presence of tryptophan and its position along with lysine and then peptide conjugation with 2 different chain lengths of poly glutamate may influence the cellular uptake and cytotoxicity of the drug.

The cytotoxicity of the synthesized CPPs and the corresponding nanoparticles (-E4 and -E8) was investigated as a function of concentrations at two incubation times of 24 (supplementary data, Figure S2) and 48 h (Figure 2). As illustrated in Figure 2a, (KW)5 showed the lowest cytotoxicity at concentration of 5 µM. At the concentration of 10 µM, the lowest cytotoxicity was obtained by K2W4K2 and K3W4K3 and at 25 µM, the lowest cytotoxicity belonged to (KW)5 and K3W4K3. Taken all data together, it was shown that increasing the number of amino acids could result in decreased cytotoxicity so that the peptides with 10 amino acids

(higher number of amino acids) exhibited lower toxicity than peptides composed of 8 amino acids (lower number of amino acids). Displacement of lysine and tryptophan had impact on CPPs cytotoxicity since they showed different cytotoxicities. However, it cannot be concluded that the alternative design is better than the block design or vice versa. Binding of E4 (Figure 2b) and E8 (Figure 2c) to the peptides led to a significant decrease in the cytotoxicity. Interestingly, CPPs-E8 nanoparticles showed even lower cytotoxicity than CPPs-E4 nanoparticles. It indicates that poly glutamate chain length can be considered as an important factor in cytotoxicity and increasing the chain length (in range of study, from 4 to 8) leads to a significant decrease in cytotoxicity.

Cellular uptake of the synthesized CPPs labeled with FITC (FITC-CPPs) and the corresponding nanoparticles (FITC-CPPs-E8 nanoparticles) in MCF-7 cells was first investigated by fluorescence microscopy and then the uptake efficiency was obtained by flow cytometry. Based on the fluorescence microscopy images, the green fluorescence of FITC existed inside the cells even at the lowest concentration (10 μM). It is indicated that the peptides and nanoparticles possess a good ability for entering the MCF-7 cells. Increasing the concentration from 10 μM (Figure 3a) to 25 μM (Figure 3) or the highest concentration of 50 μM (supplementary data, Figure S3) led to a clear increase in cellular uptake for both CPPs and nanoparticles which is an indicative of the significant role of concentration. Besides, it was shown that CPPs and CPPs-E8 nanoparticles of K3W4K3, W3K4W3, [KW]5 and [KW]4 accumulated in the nucleus of the cells that is an indicative of their ability to pass other barriers inside the cells and reaching the nucleus, while K2W4K2 peptide and its corresponding nanoparticle localized in the cytoplasm. There are different uptake pathways for penetrating of the CPPs to the cells and it depends on different factors including peptide concentration, peptide sequence (structure, length and charge), and lipid composition [43]. K2W4K2 might be translocated by a different internalization mechanism from the other

peptides. The probable mechanism for this peptide might be the caveolin pathway [44]. It was reported that accumulation of the caveolins in the endoplasmic reticulum leads to an apparent concentration of the proteins in lipid droplets [45]. Hence, it is possible that K2W4K2 may be associated with lipid droplets or other cytoplasmic particles and this peptide might need longer time to enter to the nucleus [44]. Both peptide and–E8 nanoparticle of W2K4W2 displayed the lowest fluorescence inside the cells which is possibly due to its low cellular uptake, which means its weak internalization into the cells.

Based on the flow cytometry results, the uptake was concentration dependent for all of the CPPs and nanoparticles and increased with increasing the concentration up to 25 µM (Figure 4). At this concentration the cell fluorescence reached the maximum percentage (about 100%) for all of the CPPs except W2K4W2 (Figure 4d) which was as low as 20%. By increasing the concentration from 25 µM to 50 µM, the cell fluorescence remained stable (at plateau) for K3W4K3 (Figure 4a), W3K4W3 (Figure 4b) and K2W4K2 (Figure 4c); however, the cell fluorescence decreased to about 75% for (KW)4 and (KW)5 (Figure 4e and 4f, respectively). For all of the nanoparticles (Figure 4), cellular uptake was lower in comparison with their corresponding CPPs at the concentration of 10 µM and 25 µM. The fluorescent signal of K3W4K3-E8 (Figure 4a), K2W4K2-E8 (Figure 4b) and W3K4W3-E8 (Figure 4c) reached the same percentage with the corresponding CPPs (100%) at the concentration of 50 µM and there was no significant difference between each of the mentioned CPPs and its nanoparticle at this concentration. Cellular uptake of (KW)4-E8 (Figure 4e) and (KW)5-E8 (Figure 4f) was obtained significantly higher (uptake of 90%) in comparison with their corresponding CPPs (uptake of 75%) at the concentration of 50 µM. Although, the cell uptake of W2K4W2-E8 (Figure 4d) was significantly higher than its corresponding CPP (W2K4W2) at the concentrations of 25 µM and 50 µM, it still exhibited the lowest percentage of cellular uptake compared to all other CPPs-E8 nanoparticles which

is in agreement with the result of fluorescence microscopy. It was reported that the addition of tryptophan amino acid could improve cellular uptake efficiency and peptides with sequences containing tryptophans in the middle or along the peptide sequence resulted in high uptake [40]. Interestingly, it was obtained that the cytotoxicity decreased markedly and the cellular uptake increased partly following the coupling of E8 and E4 to CPPs and synthesizing the nanoparticles. CPPs –E8 showed less cytotoxicity and more improved delivery of EPR compared to CPPs –E4. CPPs present a great diversity in terms of amino acid composition and 3D structure, with examples of cationic, anionic, and neutral sequences showing varying degrees of hydrophobicity and polarity. The various CPPs sequences may lead to different modes of cellular uptake, and different levels of uptake. CPPs can traverse membranes in order to enter cells via different uptake mechanisms. Despite many studies on CPPs, the mechanisms by which CPPs enter the cells have not been completely understood. For a long time, it was believed that CPPs would most likely enter cells by a passive process, which is temperature and receptor independent [46]. Endocytosis, being the most common process used by cells to absorb materials from their environment, can also be used as the translocation pathway of CPPs into cells [46, 47]. Endocytosis is a generic term for several different processes, such as phagocytosis for large particles and pinocytosis for smaller ones, as well as receptor-mediated endocytosis in which clathrin or caveolin pits are involved [24, 43, 46]. Several receptors were uncovered to be involved in internalization of CPPs, such as chemokine receptors, syndecans [48, 49], neuropilins [50, 51], the family of integrins [52], homing sequences, and positively-charged scavenger receptors [53, 54]. Micropinocytosis appears to be another pathway for some of CPPs. that is mediated by positively charged residues interacting with phosphoinositides. A nonendocytotic, receptor-free, energy-independent cellular process is another mechanism of the CPP translocation across biologic membranes, including formation of inverted micelles, direct translocation through the lipid

bilayer, and pore formation on the membrane [46, 47, 55, 56]. CPPs with high content in cationic residues are first absorbed at the cell surface to the numerous anionic moieties, such as sialic or phospholipidic acid or heparan sulfate proteoglycans [46, 57]. Which of these mechanisms a CPP will use is dependent on such parameters as concentration, size (with cargo), temperature, cell type, and modifications of CPPs or their cargo [43, 46, 55].

The cell membrane is a heterogeneous double layer where some regions are denser and some others have more fluidity due to the presence of different lipid compositions. These properties in turn along with CPPs' properties can result in a variety of signaling pathways and different levels and modes of uptake which depend upon the conditions used for testing CPPs [58, 59, 60, 61, 62]. Since the synthesized amphipathic peptides commonly have positive charge and cancer cell membranes typically carry a net negative charge [63], the elevated expression of anionic molecules such as proteoglycans [64] and the electrostatic attraction between them is believed to play a conclusive role in the cellular uptake of this peptides. Different studies indicated that endocytosis and direct translocation through the cellular membrane are the major mechanisms used by CPPs to gain entry into the cell [30].

To determine if the synthesized peptides and nanoparticles can be utilized for the delivery of biologically relevant doses of EPR to cells, EPR was conjugated to these synthesized peptides using succinyl hydrolysable spacer which allows the drug to release after the uptake into the cells [65]. The antitumor activity of free drug (EPR) was then examined and compared to CPPs-EPR conjugates and CPPs-E8-EPR nanoparticles at various concentrations in MCF-7 cells. As demonstrated in Figure 6, anti-proliferative activity was concentration dependent which increased by an increase in the concentration of CPP-EPR. Moreover, incubation time also led to higher anti-proliferative activity. Following the conjugation of EPR to the CPPs, CPPs-E4 and CPPs-E8 nanoparticles, the anti-proliferative activity of the drug increased significantly at the highest concentration (25 μM). Free drug (EPR) showed 63% anti-

proliferative activity. The antitumor activity increased to 63%-79% and 87%-91% (Figure 6a and S3a) for all CPPs-EPR conjugates at 25 µM at the respective incubation time of 24 and 48 h. It can be concluded that at the highest concentration, peptides improves the antitumor activity of EPR in comparison to free EPR. The enhanced antitumor activity of CPPs-EPR conjugates in comparison with free EPR can be related to their high cellular uptake tendency. Among all CPP-EPR conjugates at 25 µM, K3W4K3-EPR exhibited the highest anti-proliferative activity and W2K4W2-EPR as well as (KW)4-EPR possessed the lowest anti-proliferative activity after 24 h incubation. Following the increase in incubation time to 48 h, K3W4K3-EPR and W2K4W2-EPR showed the highest and the lowest anti-proliferative activity), respectively (Figure 6a). The lowest antitumor activity of W2K4W2-EPR can be due to its lowest cellular uptake demonstrated by both fluorescence microscopy and flow cytometry. CPPs-EPR-nanoparticles displayed higher anti-proliferative activity compared to free EPR and also CPPs-EPR conjugates at both incubation times especially at higher concentrations while overall they showed very low cytotoxicity even at the highest concentration. Therefore, their enhanced anti-proliferative activity is possibly related to their high cellular uptake tendency. Among all CPPs-EPR-nanoparticles, CPPs–E8-EPR (Figure S5c (supplementary data) and Figure 6c) showed higher anti-proliferative activity than CPPs–E4-EPR (Figure S5b (supplementary data) and Figure 6b) at both incubation times. As illustrated in Figure 6c, K3W4K3-E8-EPR nanoparticles exhibited the highest anti-proliferative activity (92%) of all CPPs-E8-EPR at 25 µM following incubation for 48 h. Furthermore, K3W4K3-E8 showed the lowest cytotoxicity of among all products produced in the present study. Generally, CPPs and CPPs-E4 or –E8 nanoparticles displayed improved anti-proliferative activity compared to free EPR (at higher concentrations). This enhanced antitumor activity could be attributed to the high cellular uptake tendency of the synthesized peptides or nanoparticles [66]. Nanoparticles showed greater intracellular uptake and less

cytotoxicity. Moreover, the effect of EPR was better for nanoparticles compared to CPPs at higher concentration levels. The reason for this may be due to the changes in conformation and the charge of peptides of nanoparticles and diverse uptake pathways following an interaction with cell membrane.

It was reported that the endocytosis pathway may be responsible for the vast majority of cationic peptide internalization at low concentrations. It was shown that at low concentration, endocytosis of peptides could occur which may result in endosomal entrapped peptides and possible metabolic degradation [67, 68]. However numerous evidences suggest that direct penetration does occur at high concentrations (above 10 μm) [67, 68]. Pathways of the uptake depended concentration can explain variation of cytotoxicity and uptake of peptides. As shown, the uptake of peptides and following antitumor activity of EPR-CPPs and EPR-CPPs-E8 increased at high concentrations and this can possibly due to direct translocation at high concentration.

5. Conclusion

In summary, different linear peptides were successfully synthesized separately or conjugated to EPR. Poly glutamate (E4 or E8) was also conjugated to the peptides and peptides-EPR to prepare nanoparticles. The effect of various CPPs and their nanoparticles was then evaluated against a breast cancer cell line (MCF-7). Results showed that cytotoxicity was concentration and time dependent. Binding of poly glutamate to CPPs resulted in a significant decrease in cytotoxicity. Interestingly, CPPs-E8 nanoparticles showed lower cytotoxicity than CPPs-E4. Uptake was concentration dependent for all of the CPPs and nanoparticles up to 25 μM. Among all of the CPPs, W2K4W2 exhibited the lowest uptake. K3W4K3-E8, K2W4K2-E8 and W3K4W3-E8 reached the highest uptake at the concentration of 50 μM and there was no significant difference between each of them and their nanoparticles. Following the conjugation of EPR to the CPPs and nanoparticles, the anti-proliferative activity of EPR

increased significantly at the highest concentration (25 µM). CPPs-EPR-nanoparticles displayed higher anti-proliferative activity compared to CPPs-EPR conjugates especially at 25 µM. Interestingly, CPPs–E8-EPR nanoparticles showed higher anti-proliferative activity than CPPs–E4-EPR. K3W4K3-E8-EPR nanoparticles exhibited the lowest cytotoxicity, high cellular uptake and the highest anti-proliferative activity at 25 µM following 48h incubation. Taking together the aforementioned advantages, the peptide nanoparticles are proposed as more potential nanosystems for cellular delivery of drugs at high concentration levels compared to CPPs, but they should also be tested *in-vivo*.

Funding

The financial support from the "Drug Applied Research Center", Tabriz University of Medical Sciences is greatly acknowledged. This paper is based on the MSc thesis submitted by Samaneh Mohammadi in the Faculty of Advanced Medical Sciences, Tabriz University of Medical Sciences.

Disclosure statement

The authors declare that there is no conflict of interest. The authors alone are responsible for the content and writing of the paper.

References

1. Dissanayake S, Denny WA, Gamage S, et al. Recent developments in anticancer drug delivery using cell penetrating and tumor targeting peptides. Journal of Controlled Release. 2017.

2. Wang H, Sun M, Li D, et al. Redox sensitive PEG controlled octaarginine and targeting peptide co-modified nanostructured lipid carriers for enhanced tumour penetrating and targeting in vitro and in vivo. Artificial Cells, Nanomedicine, and Biotechnology. 2017:1-10.

3. Han C, Li Y, Sun M, et al. Small peptide-modified nanostructured lipid carriers distribution and targeting to EGFR-overexpressing tumor in vivo. Artificial cells, nanomedicine, and biotechnology. 2014;42(3):161-166.

4. Yu M, Han S, Kou Z, et al. Lipid nanoparticle-based co-delivery of epirubicin and BCL-2 siRNA for enhanced intracellular drug release and reversing multidrug resistance. Artificial Cells, Nanomedicine, and Biotechnology. 2017:1-10.

5. Plosker GL, Faulds D. Epirubicin. Drugs. 1993;45(5):788-856.

6. Robert J. Clinical pharmacokinetics of epirubicin. Clinical pharmacokinetics. 1994;26(6):428-438.

7. Charak S, Jangir DK, Tyagi G, et al. Interaction studies of Epirubicin with DNA using spectroscopic techniques. Journal of Molecular Structure. 2011;1000(1):150-154.

8. Launchbury AP, Habboubi N. Epirubicin and doxorubicin: a comparison of their characteristics, therapeutic activity and toxicity. Cancer treatment reviews. 1993;19(3):197-228.

9. Beslija S. The role of anthracyclines/anthraquinones in metastatic breast cancer. Breast cancer research and treatment. 2003;81:25-32.

10. Ormrod D, Holm K, Goa K, et al. Epirubicin. Drugs & aging. 1999;15(5):389-416.

11. Coukell AJ, Faulds D. Epirubicin. Drugs. 1997;53(3):453-482.

12. Nasrolahi Shirazi A, Tiwari R, Chhikara BS, et al. Design and biological evaluation of cell-penetrating peptide–doxorubicin conjugates as prodrugs. Molecular pharmaceutics. 2013;10(2):488-499.

13. Yang X, Deng W, Fu L, et al. Folate-functionalized polymeric micelles for tumor targeted delivery of a potent multidrug-resistance modulator FG020326. Journal of Biomedical Materials Research Part A. 2008;86(1):48-60.

14. Chavanpatil MD, Khdair A, Gerard B, et al. Surfactant–polymer nanoparticles overcome P-glycoprotein-mediated drug efflux. Molecular pharmaceutics. 2007;4(5):730-738.

15. Sadava D, Coleman A, Kane SE. Liposomal daunorubicin overcomes drug resistance in human breast, ovarian and lung carcinoma cells. Journal of liposome research. 2002;12(4):301-309.

16. Lindgren M, Rosenthal-Aizman K, Saar K, et al. Overcoming methotrexate resistance in breast cancer tumour cells by the use of a new cell-penetrating peptide. Biochemical pharmacology. 2006;71(4):416-425.

17. Dhankhar R, Vyas SP, Jain AK, et al. Advances in novel drug delivery strategies for breast cancer therapy. Artificial Cells, Blood Substitutes, and Biotechnology. 2010;38(5):230-249.

18. Wang X, Low XC, Hou W, et al. Epirubicin-adsorbed nanodiamonds kill chemoresistant hepatic cancer stem cells. ACS nano. 2014;8(12):12151-12166.

19. Hu L, Jia Y. Preparation and characterization of solid lipid nanoparticles loaded with epirubicin for pulmonary delivery. Die Pharmazie-An International Journal of Pharmaceutical Sciences. 2010;65(8):585-587.

20. Lo Y-L. Phospholipids as multidrug resistance modulators of the transport of epirubicin in human intestinal epithelial Caco-2 cell layers and everted gut sacs of rats. Biochemical pharmacology. 2000;60(9):1381-1390.

21. Yang Q, Wang X-d, Chen J, et al. A clinical study on regional lymphatic chemotherapy using an activated carbon nanoparticle–epirubicin in patients with breast cancer. Tumor Biology. 2012;33(6):2341-2348.

22. Birnbaum DT, Brannon-Peppas L. Molecular weight distribution changes during degradation and release of PLGA nanoparticles containing epirubicin HCl. Journal of Biomaterials Science, Polymer Edition. 2003;14(1):87-102.

23. Sahu KK, Minz S, Kaurav M, et al. Proteins and peptides: The need to improve them as promising therapeutics for ulcerative colitis. Artificial cells, nanomedicine, and biotechnology. 2016;44(2):642-653.

24. Farkhani SM, Valizadeh A, Karami H, et al. Cell penetrating peptides: efficient vectors for delivery of nanoparticles, nanocarriers, therapeutic and diagnostic molecules. Peptides. 2014;57:78-94.

25. Langel U. Handbook of cell-penetrating peptides. CRC press; 2006.

26. Kristensen M, Nielsen HM. Cell-penetrating peptides as tools to enhance non-injectable delivery of biopharmaceuticals. Tissue Barriers. 2016;4(2):e1178369.

27. Jin C, Bai L, Lin L, et al. Paclitaxel-loaded nanoparticles decorated with bivalent fragment HAb18 F (ab') 2 and cell penetrating peptide for improved therapeutic effect on hepatocellular carcinoma. Artificial Cells, Nanomedicine, and Biotechnology. 2017:1-9.

28. Clavier S, Du X, Sagan S, et al. An integrated cross-linking-MS approach to investigate cell penetrating peptides interacting partners. EuPA Open Proteomics. 2014;3:229-238.

29. Figueiredo IR, Freire JM, Flores L, et al. Cell-penetrating peptides: A tool for effective delivery in gene-targeted therapies. IUBMB life. 2014;66(3):182-194.

30. Milletti F. Cell-penetrating peptides: classes, origin, and current landscape. Drug discovery today. 2012;17(15):850-860.

31. Heitz F, Morris MC, Divita G. Twenty years of cell-penetrating peptides: from molecular mechanisms to therapeutics. British journal of pharmacology. 2009;157(2):195-206.

32. Najafi-Hajivar S, Zakeri-Milani P, Mohammadi H, et al. Overview on experimental models of interactions between nanoparticles and the immune system. Biomedicine & Pharmacotherapy. 2016;83:1365-1378.

33. Niazi M, Zakeri-Milani P, Najafi Hajivar S, et al. Nano-based strategies to overcome p-glycoprotein-mediated drug resistance. Expert opinion on drug metabolism & toxicology. 2016;12(9):1021-1033.

34. Mussa Farkhani S, Asoudeh Fard A, Zakeri-Milani P, et al. Enhancing antitumor activity of silver nanoparticles by modification with cell-penetrating peptides. Artificial cells, nanomedicine, and biotechnology. 2017;45(5):1029-1035.

35. Dubikovskaya EA, Thorne SH, Pillow TH, et al. Overcoming multidrug resistance of small-molecule therapeutics through conjugation with releasable octaarginine transporters. Proceedings of the National Academy of Sciences. 2008;105(34):12128-12133.

36. Mohammadi S, Mojarrad JS, Zakeri-Milani P, et al. Synthesis and In Vitro Evaluation of Amphiphilic Peptides and Their Nanostructured Conjugates. Advanced pharmaceutical bulletin. 2015;5(1):41.

37. Kim J-K, Anderson J, Jun H-W, et al. Self-assembling peptide amphiphile-based nanofiber gel for bioresponsive cisplatin delivery. Molecular pharmaceutics. 2009;6(3):978-985.

38. Nasrolahi Shirazi A, Oh D, Tiwari RK, et al. Peptide amphiphile containing arginine and fatty acyl chains as molecular transporters. Molecular pharmaceutics. 2013;10(12):4717-4727.

39. Gautam A, Singh H, Tyagi A, et al. CPPsite: a curated database of cell penetrating peptides. Database. 2012;2012:bas015.

40. Rydberg HA, Matson M, Åmand HL, et al. Effects of tryptophan content and backbone spacing on the uptake efficiency of cell-penetrating peptides. Biochemistry. 2012;51(27):5531-5539.

41. Farkhani SM, Johari-ahar M, Zakeri-Milani P, et al. Enhanced cellular internalization of CdTe quantum dots mediated by arginine-and tryptophan-rich cell-penetrating peptides as efficient carriers. Artificial cells, nanomedicine, and biotechnology. 2016;44(6):1424-1428.

42. Zakeri-Milani P, Farkhani SM, Shirani A, et al. CELLULAR UPTAKE AND ANTI-TUMOR ACTIVITY OF GEMCITABINE CONJUGATED WITH NEW AMPHIPHILIC CELL PENETRATING PEPTIDES.

43. Madani F, Lindberg S, Langel Ü, et al. Mechanisms of cellular uptake of cell-penetrating peptides. Journal of Biophysics. 2011;2011.

44. Zaro JL, Vekich JE, Tran T, et al. Nuclear localization of cell-penetrating peptides is dependent on endocytosis rather than cytosolic delivery in CHO cells. Molecular pharmaceutics. 2009;6(2):337-344.

45. Ostermeyer AG, Paci JM, Zeng Y, et al. Accumulation of caveolin in the endoplasmic reticulum redirects the protein to lipid storage droplets. The Journal of cell biology. 2001;152(5):1071-1078.

46. Durzyńska J, Przysiecka Ł, Nawrot R, et al. Viral and other cell-penetrating peptides as vectors of therapeutic agents in medicine. Journal of Pharmacology and Experimental Therapeutics. 2015;354(1):32-42.

47. S Choi Y, E David A. Cell penetrating peptides and the mechanisms for intracellular entry. Current pharmaceutical biotechnology. 2014;15(3):192-199.

48. Letoha T, Keller-Pintér A, Kusz E, et al. Cell-penetrating peptide exploited syndecans. Biochimica et Biophysica Acta (BBA)-Biomembranes. 2010;1798(12):2258-2265.

49. Kawaguchi Y, Takeuchi T, Kuwata K, et al. Syndecan-4 is a receptor for clathrin-mediated endocytosis of arginine-rich cell-penetrating peptides. Bioconjugate chemistry. 2016;27(4):1119-1130.

50. Prud'homme GJ, Glinka Y. Neuropilins are multifunctional coreceptors involved in tumor initiation, growth, metastasis and immunity. Oncotarget. 2012;3(9):921.

51. Pang H-B, Braun GB, Ruoslahti E. Neuropilin-1 and heparan sulfate proteoglycans cooperate in cellular uptake of nanoparticles functionalized by cationic cell-penetrating peptides. Science advances. 2015;1(10):e1500821.

52. Mokhtarieh AA, Kim S, Lee Y, et al. Novel cell penetrating peptides with multiple motifs composed of RGD and its analogs. Biochemical and biophysical research communications. 2013;432(2):359-364.

53. Reissmann S. Cell penetration: scope and limitations by the application of cell-penetrating peptides. Journal of Peptide Science. 2014;20(10):760-784.

54. Juks C, Lorents A, Arukuusk P, et al. Cell-penetrating peptides recruit type A scavenger receptors to the plasma membrane for cellular delivery of nucleic acids. The FASEB Journal. 2017;31(3):975-988.

55. Lindgren M, Langel Ü. Classes and prediction of cell-penetrating peptides. Cell-penetrating peptides: Methods and protocols. 2011:3-19.

56. Thorén PE, Persson D, Lincoln P, et al. Membrane destabilizing properties of cell-penetrating peptides. Biophysical chemistry. 2005;114(2):169-179.

57. Pujals S, Fernández-Carneado J, López-Iglesias C, et al. Mechanistic aspects of CPP-mediated intracellular drug delivery: relevance of CPP self-assembly. Biochimica et Biophysica Acta (BBA)-Biomembranes. 2006;1758(3):264-279.

58. Jacobson K, Mouritsen OG, Anderson RGW. Lipid rafts: at a crossroad between cell biology and physics. Nature cell biology. 2007;9(1):7-14.

59. Simons K, Sampaio JL. Membrane organization and lipid rafts. Cold Spring Harbor perspectives in biology. 2011;3(10):a004697.

60. Simons K, Ehehalt R. Cholesterol, lipid rafts, and disease. The Journal of clinical investigation. 2002;110(110 (5)):597-603.

61. McMahon HT, Gallop JL. Membrane curvature and mechanisms of dynamic cell membrane remodelling. Nature. 2005;438(7068):590-596.

62. van Meer G, de Kroon AIPM. Lipid map of the mammalian cell. Journal of cell science. 2011;124(1):5-8.

63. Schweizer F. Cationic amphiphilic peptides with cancer-selective toxicity. European journal of pharmacology. 2009;625(1):190-194.

64. Ziegler A, Seelig J. Binding and clustering of glycosaminoglycans: a common property of mono-and multivalent cell-penetrating compounds. Biophysical journal. 2008;94(6):2142-2149.

65. Cavallaro G, Mariano L, Salmaso S, et al. Folate-mediated targeting of polymeric conjugates of gemcitabine. International journal of pharmaceutics. 2006;307(2):258-269.

66. Aroui S, Brahim S, Waard MD, et al. Cytotoxicity, intracellular distribution and uptake of doxorubicin and doxorubicin coupled to cell-penetrating peptides in different cell lines: a comparative study. Biochemical and biophysical research communications. 2010;391(1):419-425.

67. Brock R. The uptake of arginine-rich cell-penetrating peptides: Putting the puzzle together. Bioconjugate chemistry. 2014;25(5):863-868.

68. Mellert K, Lamla M, Scheffzek K, et al. Enhancing endosomal escape of transduced proteins by photochemical internalisation. PloS one. 2012;7(12):e52473.

Table 1. Different cell penetrating peptide amphiphiles (CPPs) synthesized in the present study

CPPs	Sequence design	Number of amino acids	Design
(KW)4	KWKWKWKW	8	Alternative
(KW)5	KWKWKWKWKW	10	Alternative
K2W4K2	KKWWWWKK	8	Two-block
K3W4K3	KKKWWWWKKK	10	Tri-block
W2K4W2	WWKKKKWW	8	Two-block
W3K4W3	WWWKKKKWWW	10	Tri-block

Note: W and K represent tryptophan (hydrophobic amino acid) and lysine (charged amino acid), respectively.

Table 2. The percentage of drug (EPR) loading for different peptide-EPR conjugates (CPPs-EPR)

CPPs-EPR	Drug loading ± SD (%)
(KW)4	77.0 ± 4.2
(KW)5	74.0 ± 3.0
K2W4K2	50.2 ± 2.6
K3W4K3	58.0 ± 2.3
W2K4W2	51.0 ± 4.6
W3K4W3	61.1 ± 4.6

Note: W and K represent tryptophan (hydrophobic amino acid) and lysine (charged amino acid), respectively.

Figure captions

Figure 1. The schematic peptide synthesis of K3W4K3 (a), the schematic synthesis of FITC-labeled K3W4K3 (b) and the schematic synthesis of K3W4K3-EPR conjugate (c).

Figure 2. MTT-based cytotoxicity of different CPPs (a), CPPs-E4 nanoparticles (b) and CPPs-E8 nanoparticles (c) at various concentrations (5, 10 and 25 µM) after 48h incubation in MCF-7 cell line at 37ºC. Data represent Mean ± SD for 6 replicates.

Figure 3. Fluorescence microscopy images of MCF-7 cells incubated with FITC-labeled CPPs and their corresponding nanoparticles (CPPs-E8) at concentration of 10 (a) and 50 (b) µM after 2h incubation at 37ºC.

Figure 4. Cellular uptake (%) of FITC-CPPs and the corresponding nanoparticles (FITC-CPPs-E8) at different concentration of 10, 25, and 50 µM after 2h incubation in MCF-7 cell at 37°C. Data represent Mean ± SD for 3 replicates. FITC-CPPs and FITC-CPPs-E8 nanoparticles are presented by black line with symbol of ■ and red dot line with symbol of ●, respectively.

Figure 5. Flow cytometry histograms of MCF-7 cells treated for 2 h with K3W4K3 (left) and K3W4K3-E8 (right) at various concentrations of 10 (a and d), 25 (b and e) and 50 (c and f) µM. First peak (gray color) corresponds to untreated control cells.

Figure 6. MTT-based anti-proliferative activity of different CPPs-EPR (a), CPPs-E4-EPR (b) and CPPs-E8-EPR (c) in comparison with free drug (EPR) at various concentrations (1, 5, 10 and 25 µM) after 48 h incubation in MCF-7 cells at 37º C. Data represent Mean ± SD for 6 replicates.

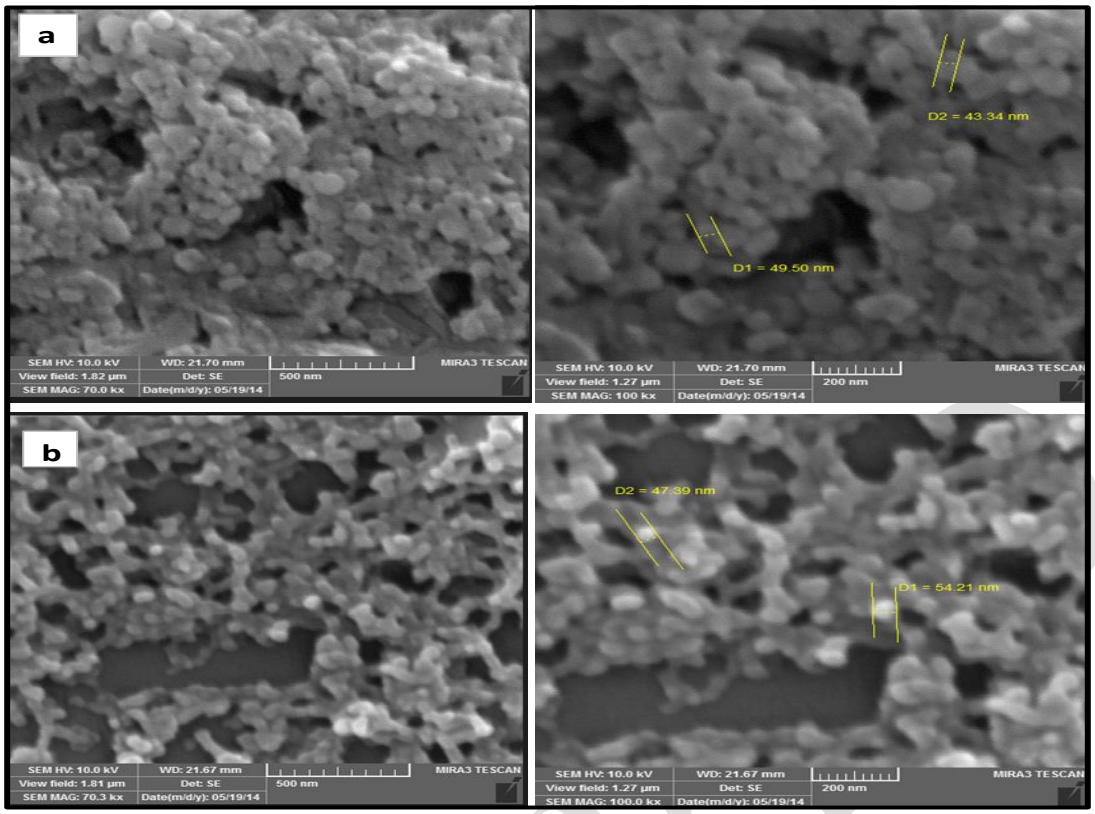

Figure 1

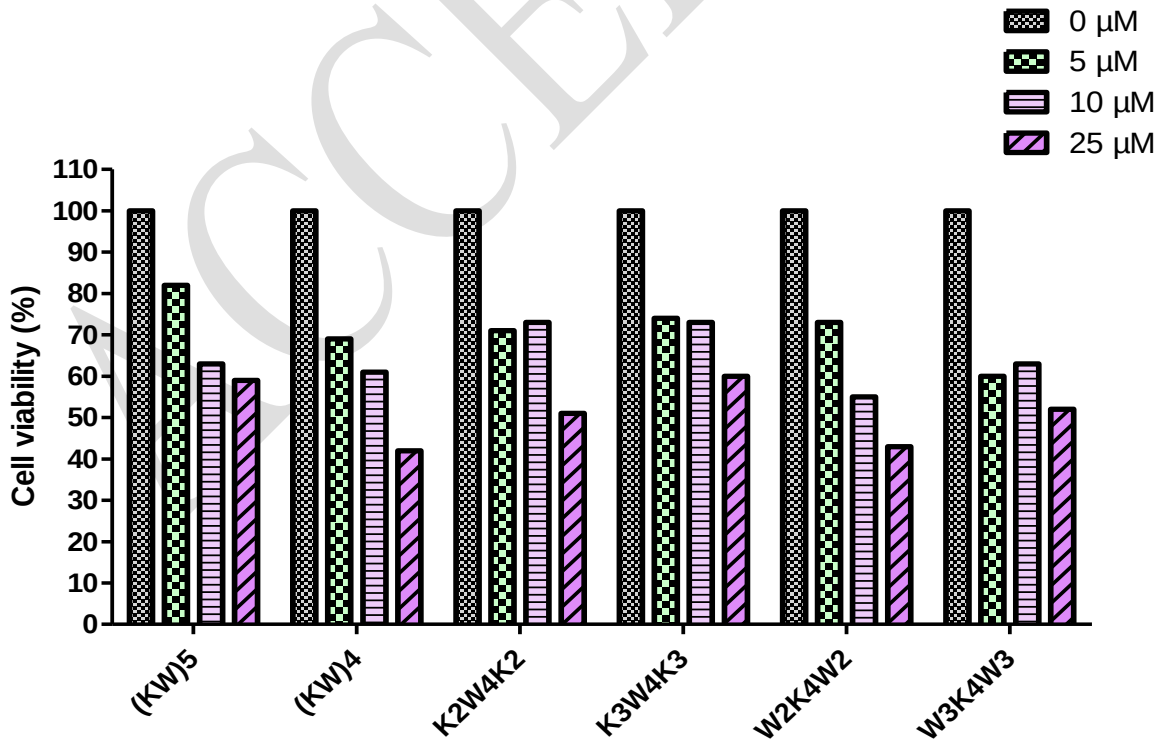

Figure 2

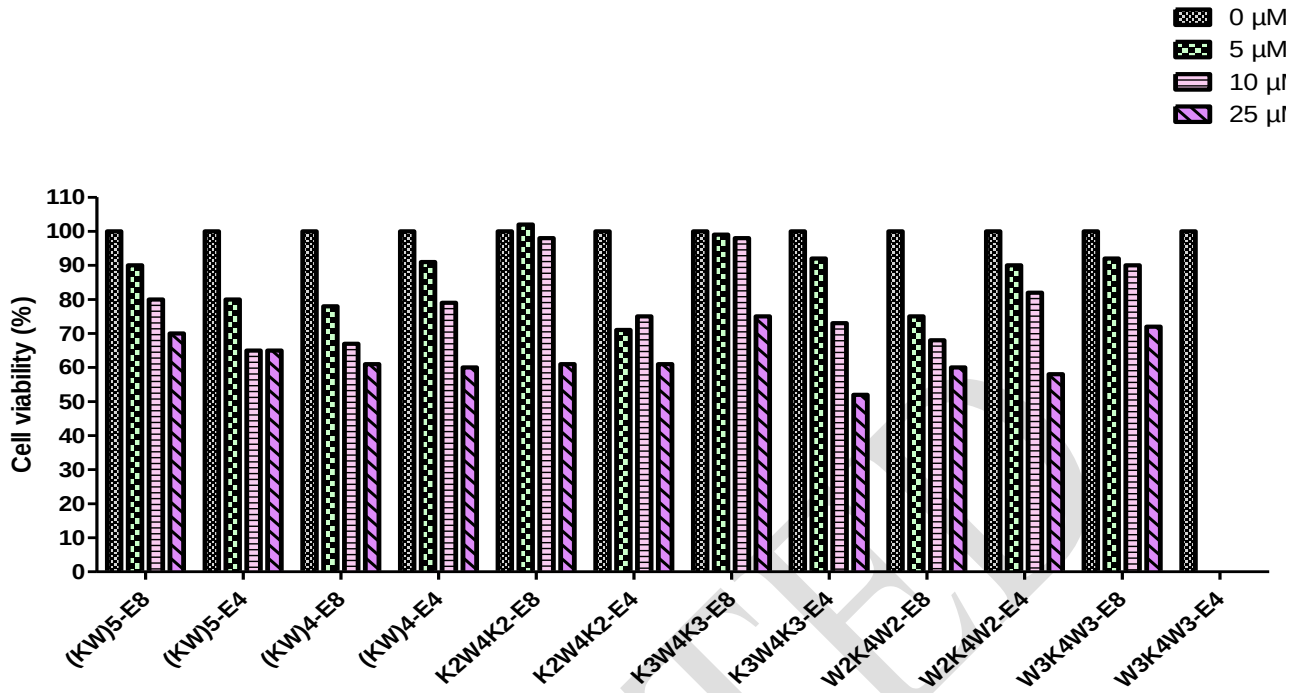

Figure 3

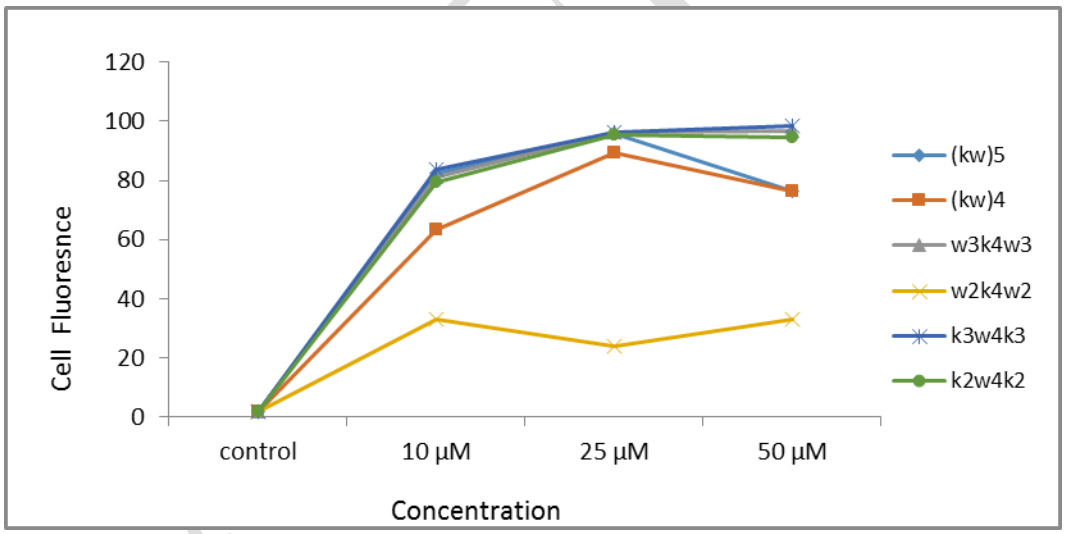

Figure 4

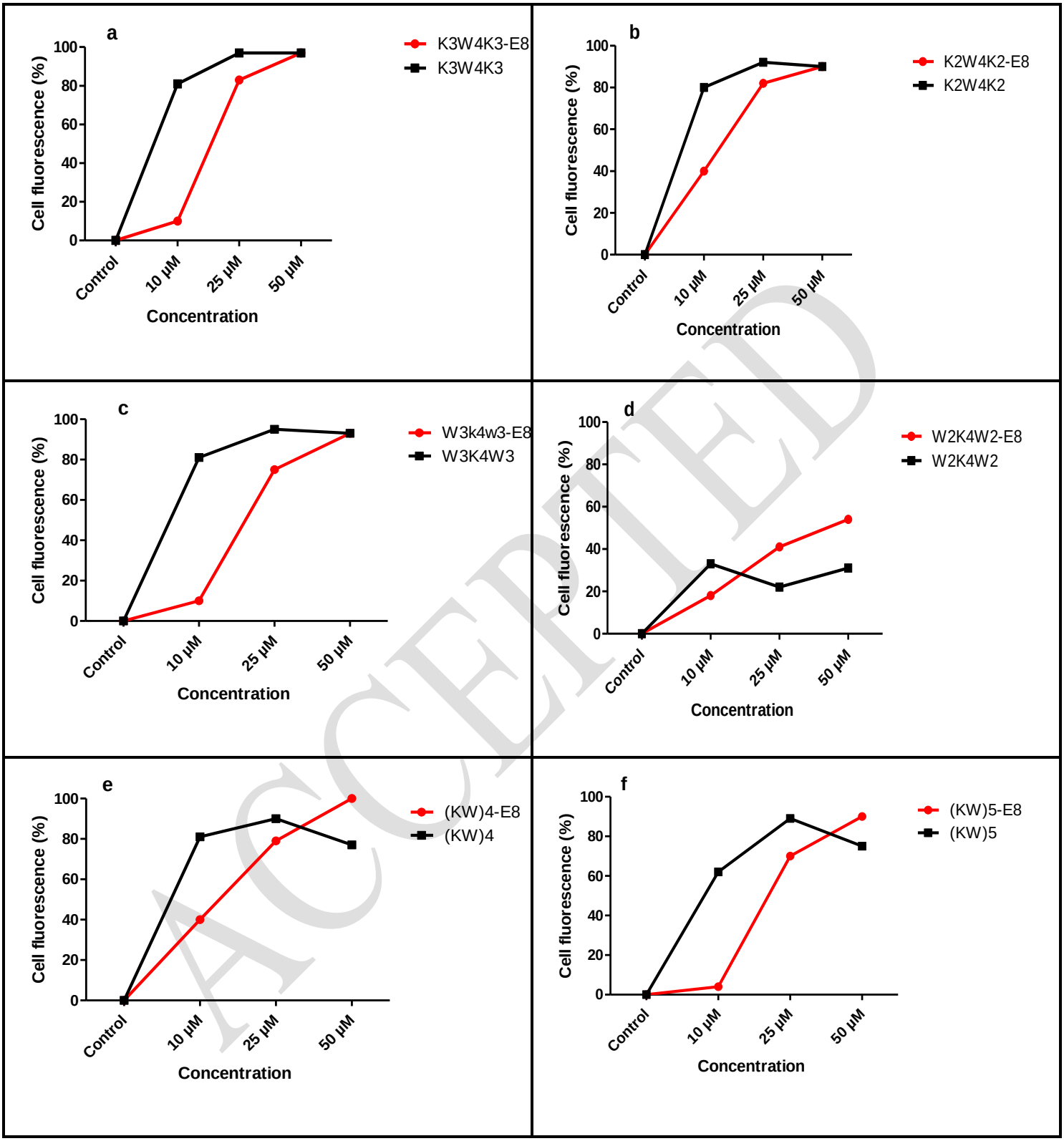

Figure 5

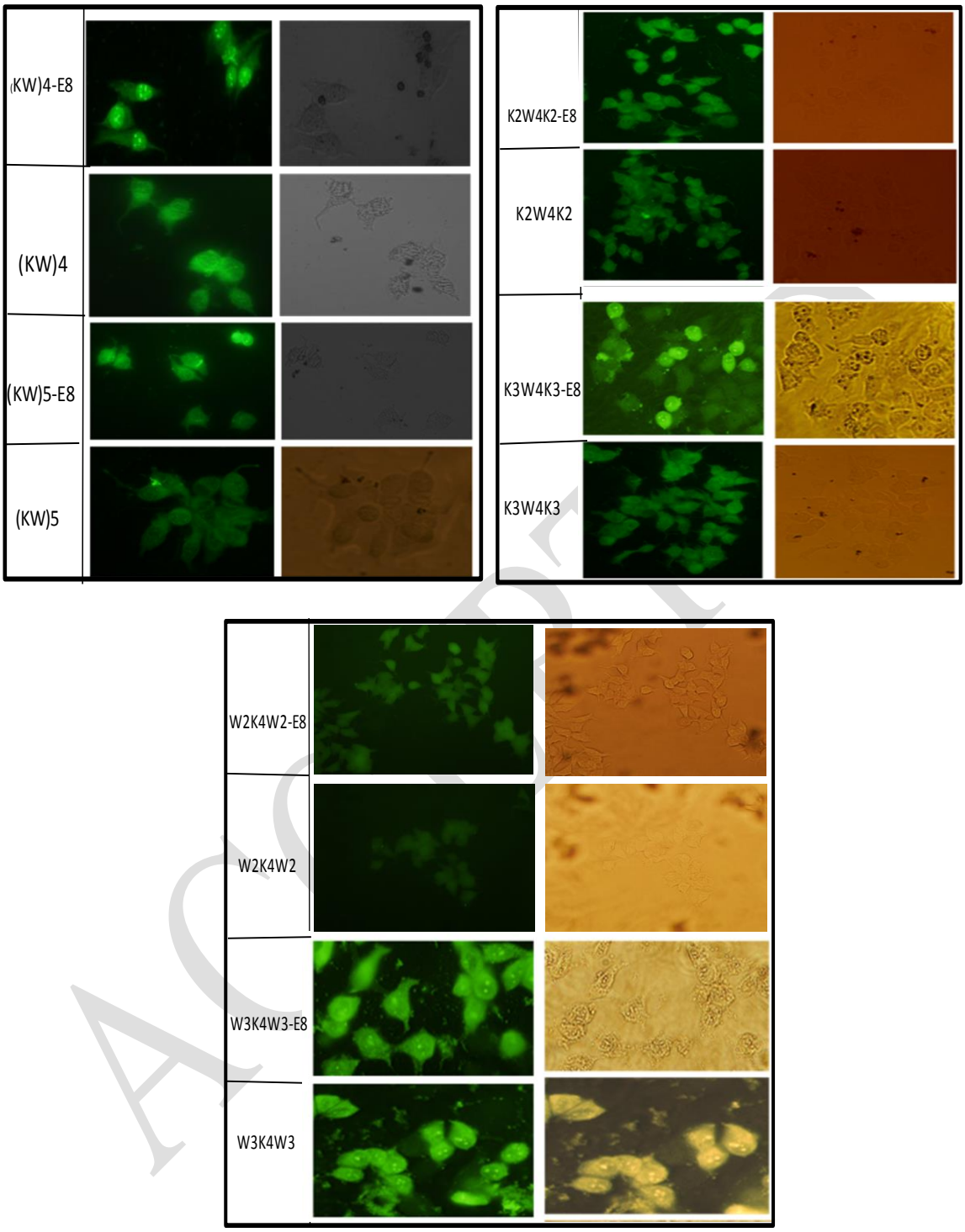
(KW)4-E8
(KW)4
(KW)5-E8
(KW)5
K2W4K2-E8
K2W4K2
K3W4K3-E8
K3W4K3
W2K4W2-E8
W2K4W2
W3K4W3-E8
W3K4W3

Figure 6

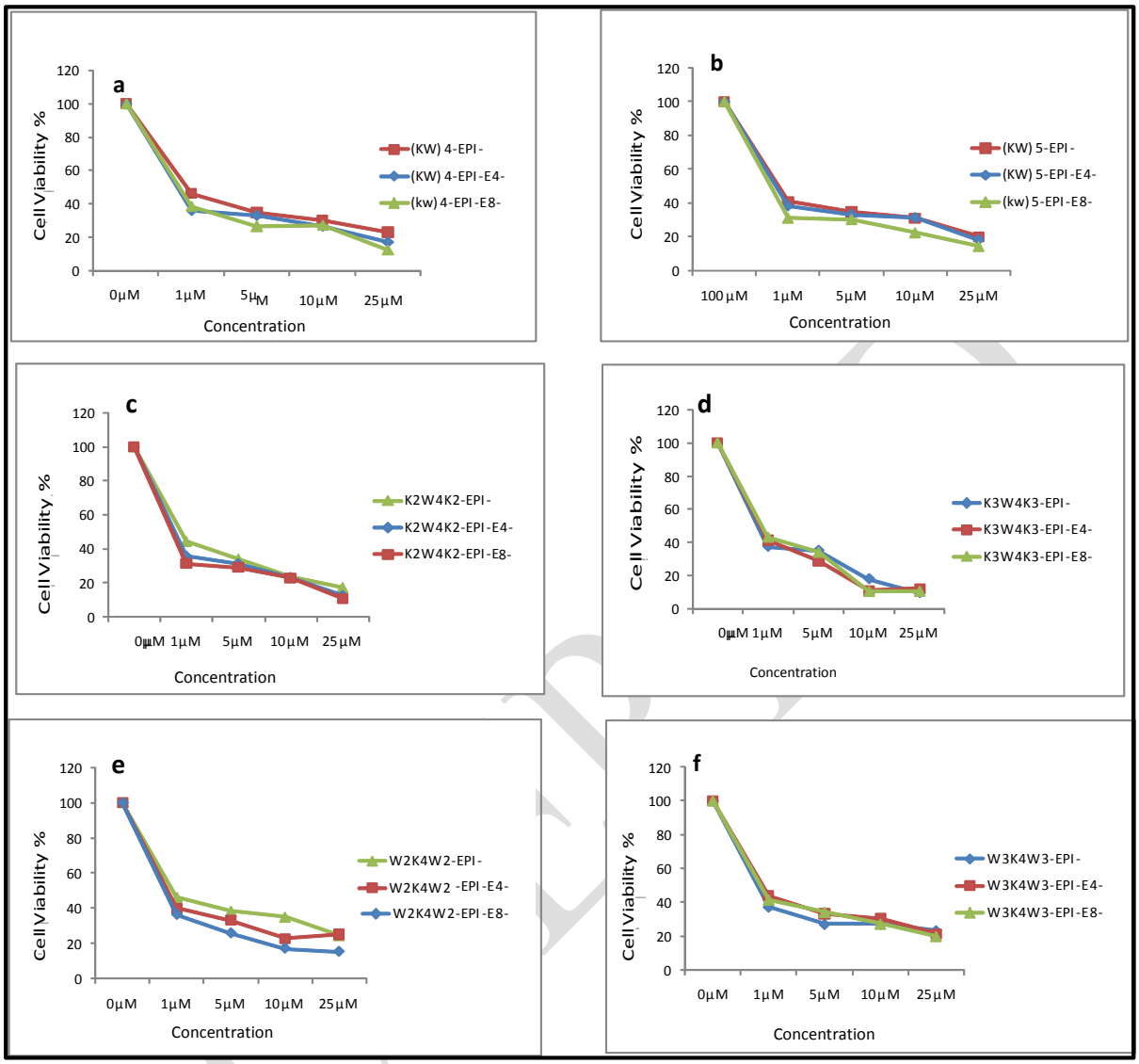
a
Cell Viability %
120
100
80
60
40
20
0
0μM 1μM 5μM 10μM 25μM
Concentration
(KW) 4-EPI-
(KW) 4-EPI-E4-
(kw) 4-EPI-E8-
b
Cell Viability %
100μM 1μM 5μM 10μM 25μM
Concentration
(KW) 5-EPI-
(KW) 5-EPI-E4-
(kw) 5-EPI-E8-
c
Cell Viability %
0μM 1μM 5μM 10μM 25μM
Concentration
K2W4K2-EPI-
K2W4K2-EPI-E4-
K2W4K2-EPI-E8-
d
Cell Viability %
0μM 1μM 5μM 10μM 25μM
Concentration
K3W4K3-EPI-
K3W4K3-EPI-E4-
K3W4K3-EPI-E8-
e
Cell Viability %
0μM 1μM 5μM 10μM 25μM
Concentration
W2K4W2-EPI-
W2K4W2 -EPI-E4-
W2K4W2-EPI-E8-
f
Cell Viability %
0μM 1μM 5μM 10μM 25μM
Concentration
W3K4W3-EPI-
W3K4W3-EPI-E4-
W3K4W3-EPI-E8-

Figure 7